Atmos. Meas. Tech. Discuss., 7, 475–507, 2014
www.atmos-meas-tech-discuss.net/7/475/2014/
doi:10.5194/amtd-7-475-2014

Atmospheric Measurement Techniques Discussions
Open Access

Continuous measurements of atmospheric water vapour isotopes in Western Siberia (Kourovka)

V. Bastrikov[1,2,3], H. C. Steen-Larsen[2], V. Masson-Delmotte[2], K. Gribanov[1], O. Cattani[2], J. Jouzel[2], and V. Zakharov[1]

[1]Ural Federal University, Ekaterinburg, 620002, Russia
[2]LSCE/IPSL, UMR8212, CEA-CNRS-UVSQ, CEA Saclay, Gif-sur-Yvette, 91191, France
[3]Institute of Industrial Ecology UB RAS, Ekaterinburg, 620219, Russia

Received: 3 October 2013 – Accepted: 9 January 2014 – Published: 21 January 2014

Correspondence to: V. Bastrikov (v.bastrikov@gmail.com)

Published by Copernicus Publications on behalf of the European Geosciences Union.

Abstract

The isotopic composition of atmospheric water vapour at the land surface has been continuously monitored at the Kourovka astronomical observatory in Western Siberia (57.037° N, 59.547° E, 300 m a.s.l.) since April 2012. These measurements provide the first record of δD, δ^{18}O and d-excess in this region. Air was sampled at 8 m height within a forest clearing. Measurements were made with a Wavelength-Scanned Cavity Ring Down Spectroscopy analyzer. A specific protocol was developed for calibration and drift corrections with a particular enhancement to ensure reliable measurements at low humidity during winter. The isotopic measurements conducted till August 2013 exhibit a clear seasonal cycle with maximum δD and δ^{18}O values in summer and minimum values in winter. In addition, considerable synoptic timescale variability of isotopic composition was observed with typical variations of 50–100 ‰ for δD, 10–15 ‰ for δ^{18}O and 2–8 ‰ for d-excess. The strong correlations between δD and local meteorological parameters (logarithm-of-humidity and temperature) are explored, with a lack of dependency in summer that points to the importance of continental recycling and local evapotranspiration. The overall correlation between δD and temperature is associated with a slope of 3 ‰ °C^{-1}. Large d-excess diurnal variability was observed during summer with up to 30 ‰ depletion during the night and the minima manifested shortly after sunrise. The accuracy of the isotopic measurements was quantified as 1.4–11.2 ‰ for δD and 0.23–1.84 ‰ for δ^{18}O depending on the humidity.

1 Introduction

The isotopic composition of atmospheric water vapour is a valuable source of information for quantifying the processes controlling the hydrological cycle. The saturation vapour pressures and air diffusivities of the natural stable isotopologues of water, $H_2{}^{16}O$, $HD^{16}O$ and $H_2{}^{18}O$, are slightly different (Merlivat and Nief, 1967; Majoube, 1971; Merlivat, 1978; Barkan and Luz, 2007; Ellehoj et al., 2013). As a result, fractionation

AMTD
7, 475–507, 2014

takes place during each phase change such as evaporation from the sea surface (Craig and Gordon, 1965; Merlivat and Jouzel, 1979), cloud formation (Dansgaard, 1964; Ciais and Jouzel, 1994), plant transpiration (Farquhar et al., 2007) and post-condensation exchange (Field et al., 2010). This fractionation therefore leads to spatial and temporal variations in the isotopic composition of atmospheric water vapour and precipitation. Thus, stable isotopes of water can be exploited as natural tracers of atmospheric transport patterns and physical processes involving water vapour in the atmosphere.

For the last several decades water isotope measurements have focused on liquid water (precipitation, surface water, soil moisture, groundwater, etc.) as a means to investigate the hydrological cycle processes (Rozanski et al., 1993; Gat, 1996). Fewer measurements of atmospheric water vapour have been made as they have previously required laborious techniques such as cryogenic sampling and subsequent isotope-ratio mass spectrometric (IRMS) analysis (Jacob and Sonntag, 1991; Han et al., 2006; Strong et al., 2007; Uemura et al., 2008).

Recently, new types of infrared laser spectrometers (Kerstel et al., 1999; Crosson et al., 2002; Baer et al., 2002) have been developed, and commercial measurement systems based on cavity ring-down (Picarro, www.picarro.com) and off-axis (Los Gatos Research, www.lgrinc.com) laser absorption spectroscopy are available. These instruments make in situ high frequency measurements of water vapour isotopic composition with an accuracy similar to that obtained by mass spectrometers (Gupta et al., 2009; Sturm and Knohl, 2010). Kerstel and Gianfrani (2008) have recently reviewed the recent advances in laser-based isotope-ratio measurements. Several intercomparison studies of different instruments have been performed (Aemisegger et al., 2012; Steen-Larsen et al., 2013). However, a range of factors like sensitivity to the level of ambient humidity and instrumental drift have led to the need for an appropriate measurement and calibration protocol (Tremoy et al., 2011; Kurita et al., 2012; Steen-Larsen et al., 2013). This need is particularly critical for measurements made at low humidity levels.

AMTD
7, 475–507, 2014

These new infrared laser spectrometers have been successfully deployed in various climates: in the Arctic (Steen-Larsen et al., 2013; Bonne et al., 2013), Europe (Aemisegger et al., 2013), Africa (Tremoy et al., 2012), and North and South America (Farlin et al., 2013; Berkelhammer et al., 2013; Galewsky et al., 2011). Within the territory of the Russian Federation, so far only precipitation isotopic data have been collected (Kurita et al., 2004) and no long-term water vapour isotope measurements have been published.

Our study is focused on the monitoring station in Western Siberia (Kourovka, Russia), providing the first isotopic record of atmospheric water vapour in this region. A Wavelength-Scanned Cavity Ring Down Spectroscopy (WS-CRDS) analyzer (Picarro Inc., Sunnyvale, CA, USA) has been installed at the Kourovka astronomical observatory, together with a meteorological station. The work is part of a project investigating the water and carbon cycles in the permafrost and pristine peatlands of Western Siberia and their projected changes associated with climate change. The first δD measurements were presented by Gribanov et al. (2013) together with the remote sensing measurements and retrievals from GOSAT, ground-based FTIR (Fourier Transform Infrared) spectra and results of the ECHAM5-wiso global circulation model. Here, we give a detailed overview of the water vapour measurement system calibration, report changes in the analytical protocol that allow accurate measurements even at very low winter humidity levels, and report the data from one year of continuous monitoring of atmospheric water vapour isotopic composition.

In Sect. 2, we describe Kourovka site characteristics, field setup and data processing protocol. In Sect. 3, we report on the instrument performance, present the calibrated data and describe the observed variability of surface water vapour isotopic composition together with a comparison with local meteorological data and analysis of the daily cycles.

AMTD
7, 475–507, 2014

2 Materials and methods

Throughout this paper, the water vapour isotopic composition is expressed in ‰ vs. the Vienna Standard Mean Ocean Water (V-SMOW; Gonfiantini, 1978) using the δ-notation (Craig, 1961). Its definition is based on the equation

$$\delta^* = (R_{\text{sample}}/R_{\text{V-SMOW}} - 1) \times 1000\,[‰], \quad (1)$$

where δ^* represents either δD or δ^{18}O and R is the ratio of one of the two stable water isotopes $^1H^2H^{16}O$ or $^1H_2{}^{18}O$ compared to $^1H_2{}^{16}O$. The second order parameter deuterium excess (hereafter noted as d-excess) is defined as the deviation from the linear relationship observed between $HD^{16}O$ and $H_2{}^{18}O$ in meteoric waters having a global mean slope of 8 (Dansgaard, 1964; Craig and Gordon, 1965):

$$\text{d-excess} = \delta D - 8 \times \delta^{18}O. \quad (2)$$

2.1 Kourovka site characteristics

Kourovka astronomical observatory (Fig. 1) was founded in 1965 as part of the Ural Federal University (the former Ural State University). It is located close to the western boundary of Western Siberia (57.037° N, 59.547° E, 300 m a.s.l.), it is surrounded by pristine peatland, and is far from any large city (~ 70 km from Ekaterinburg). There is no industry or any industrial discharge nearby. The observatory is situated in a clearing 100 × 100 m, within dense pine forest with an approximate height of 15 m. Local climate is continental. Based on published data for the region, over the past half-century the monthly mean temperatures range from −16 °C (January) to +17 °C (July) with ~ 460 mm of annual precipitation, peaking in summer (Shalaumova et al., 2010). The site is located ~ 500 km to the south of the permafrost zone.

AMTD
7, 475–507, 2014

2.2 Meteorological data

Since July 2012, a meteorological station MetPak-II (Gill Instruments Ltd., Lymington, UK) has provided high-frequency (1 Hz) continuous measurement of the following atmospheric variables: barometric pressure (±0.05 kPa), relative humidity (±0.8 % at 23 °C), air temperature (±0.1 °C), wind speed (±2 % at 12 m s^{-1}), wind direction (±3° at 12 m s^{-1}) and dew point temperature (±0.15 °C). These data are used to compare the humidity measurements performed by the isotope analyzer with meteorological measurements and to investigate the relationships between water vapour isotopic composition at the surface and local meteorological data (temperature and humidity) (see Sect. 3.8).

2.3 Isotopic measurement setup

Water vapour isotopic composition is measured with the laser spectroscopy analyzer L2130-i (Picarro Inc.) based on WS-CRDS (Brand et al., 2009; Crosson et al., 2002). The instrument was installed in Kourovka in mid-March 2012 and has been providing continuous measurements of δD and δ^{18}O since April 2012.

The analyzer is installed in an air conditioned room (temperature ~ 18 °C). A shielded air intake is installed on the roof of the building (8 m a.g.l.) and a heated ~ 6 m inlet line (O'Brien optical quality stainless steel tube, 9.5 mm (3/8 inch) OD) is connected with the analyzer. A 5 litre-per-minute pump ensures quick transport of air through the inlet tube. Electric heat tracing (type HKSI, HORST GmbH, Lorsch, Germany) maintains the temperature of the tube at ~ 60 °C.

The analyzer is programmed to perform self-calibrations after every six hours of ambient air measurement using the automated Picarro Standards Delivery Module (SDM). Each calibration is made with two reference water samples: DW (distilled water, δD = −96.4 ‰, δ^{18}O = −12.76 ‰) and YEKA (Antarctic snow and distilled water mix, δD = −289.0 ‰, δ^{18}O = −36.71 ‰). Reference waters are injected into the analyzer as water vapour with a temperature set at 140 °C mixed with dried room-air pumped

AMTD
7, 475–507, 2014

through a DRIERITE column. Adjustment of the reference water and/or dried air injection speed allows water vapour concentration to be regulated within desired limits. During calibration cycles, the humidity is usually set to 12 000 ppmv. Each reference sample is measured continuously for 30 min. A third depleted reference sample DOMEC (water standard from Laboratoire des Sciences du Climat et de l'Environnement (LSCE), δD = −424.1 ‰, δ^{18}O = −54.05 ‰) is also used periodically to assess the instrument linearity. The exact isotopic values of these reference waters were measured at LSCE by IRMS with accuracies of 0.5 ‰ for δD and 0.05 ‰ for δ^{18}O.

After each calibration, the first 13 min of ambient air measurements are discarded to ensure that any calibration water vapour is purged out of the system. The length of this period was determined during installation and found to be reasonable for our particular instrument.

Because isotopic measurements are sensitive to water vapour concentration (Steen-Larsen et al., 2013), the instrument's humidity–isotope response function was determined for the analyzer and is verified several times a year. This calibration is established by introducing reference samples at different humidity levels from 500 to 25 000 ppmv.

To improve the operation of the SDM, several improvements have been made:

- substitution of the drying column by dry air from a tank cylinder (for humidity–isotope calibration only, see Sect. 3.3);
- utilization of septa for water intake from vials with needles (to prevent bubble formation);
- replacement of ceramic syringes with glass syringes.

2.4 Data processing protocol

The data processing protocol follows the major steps described by Steen-Larsen et al. (2013). It includes the following stages:

AMTD
7, 475–507, 2014

1. raw data quality control (search and removal of random spikes, artefacts due to power supply disturbances or any other technical problems);

2. raw data flagging (for calibrations – averaging window selection in the steady plateau area, unsuccessful calibration exclusion; for air measurements – exclusion of the measurements made shortly after the instrument switching from another mode, data quality flags assignment depending on the relevant humidity level);

3. correction of the raw measurements using the humidity–isotope response functions (see Sect. 3.3);

4. conversion of the humidity-corrected measurements to the V-SMOW scale upon known reference water samples, assuming a linear instrumental drift between calibrations and bracketing a given vapour measurement (see Sect. 3.4).

5. correction of the humidity measurements using the Gill-Picarro calibration function (see Sect. 3.2).

6. averaging of the processed data over one-hour intervals.

3 Results and discussions

3.1 Instrument performance

Our Picarro isotopic analyzer has been operated continuously since April 2012 with only occasional short gaps due to electricity interruptions and minor breakdowns. Starting from June 2012, Picarro calibrations were invalidated due to a leakage in one of the Standards Delivery Module syringes. This problem led to: (1) introduction of air bubbles in SDM, (2) fractionation in the syringe because of exchange with ambient air, and (3) instabilities in injected flux and hence in the resulting measurements. The calibration

AMTD
7, 475–507, 2014

module was replaced in September 2012 using a new type of glass syringe; this led to very stable and reproducible calibrations. The data discussed in this paper is therefore limited to the one-year period starting from 21 September 2012. The earlier data starting at the beginning of the instrument's operation is limited to δD measurement. However, these limited results compare well with model estimates and FTIR measurements (Gribanov et al., 2013).

Overall, for the period from 21 September 2012 to 31 August 2013, 6794 hourly Picarro measurements have been validated, which corresponds to 82 % of the total duration (8280 h).

3.2 Humidity measurements calibration

Picarro humidity measurements (absolute humidity measured in ppmv) are compared to humidity values calculated from the Gill meteorological measurements (relative humidity and temperature) in Fig. 2. The best fit is given by a third-degree polynomial ($R^2 = 0.992$):

$$y = -168.4 + 0.823x - 2.918 \times 10^{-6}x^2 + 1.475 \times 10^{-10}x^3, \quad (3)$$

where x is the Picarro and y is the Gill humidity value (in ppmv), respectively. Equation (3) is hereafter used to translate all Picarro humidity data into the meteorological instrument scale. For the periods when the analyzer was not performing air measurements, the meteorological station humidity data are used.

Our comparison shows a non-linear correlation in the humidity range from 250 to 23 000 ppmv, best fitted by a polynomial function. In other studies, similar responses of Picarro measurements have also been observed with respect to independent meteorological device observations (Tremoy et al., 2011, in the range from 5000 to 36 000 ppmv; Bonne et al., 2013, in the range from 1000 to 18 000 ppmv). However, Aemisegger et al. (2012) showed a linear response of the analyzer when comparing to a dew point generator used to control humidity level in the range from 4000 to 31 000 ppmv.

AMTD
7, 475–507, 2014

3.3 Humidity–isotope response calibration

The Picarro analyzer humidity calibration was performed using the two water standards (DW and YEKA) during its installation and was recalibrated after the SDM replacement. The final humidity–isotope response functions in this series of measurements are shown in Fig. 3. The data are displayed for humidity levels below 5000 ppmv only, as the instrument response appears flat for higher levels. We observe different humidity dependencies for $\delta^{18}O$ measured in different water standards (green – DW standard, blue – YEKA standard) and opposite dependencies for δD. The most plausible reason for this artefact is incomplete air drying in the DRIERITE column. To confirm this hypothesis, a humidity calibration was performed with a supply of dry gas rather than gas passed through the DRIERITE. With this setup, we obtained, within uncertainties, the same calibration curves for the two standards (red – DW standard, black – YEKA standard, with one conjoint fitting line shown in red). Moreover, the overall humidity dependency became significantly less pronounced. This indicates the importance of using "dry" air with very limited residual water vapour when performing calibrations at low humidity. Table 1 gives the analytical expressions used to obtain the best fit for the humidity–isotope response function in different cases and the associated coefficients.

Note that there are no data for the DRIERITE experiments below 800 ppmv due to the technical limitations of SDM. The behaviour of the humidity–isotope response functions for these conditions is therefore unknown.

Since all periodical self-calibrations were performed using dry air generated from DRIERITE, we used the humidity–isotope response functions from Formula 1–4 (Table 1) to correct the reference water sample measurements. To correct the ambient water vapour isotope measurements, we used the humidity–isotope response functions obtained using dry air (Table 1, Formula 5–6).

AMTD
7, 475–507, 2014

3.4 Known-standard calibration

Figure 4 shows the complete set of calibrations conducted during the period from 21 September 2012 to 31 August 2013 with the V-SMOW slopes calculated from the measurements. Overall, 1672 calibrations have been made, among which 1552 (93 %) were successful (781 for DW standard and 771 for YEKA standard).

Two-standard calibrations were performed after every six hours of ambient air measurements. For each standard, the averaging window was selected within a steady plateau area, usually during the last three minutes of the half-hour measurement. Standard deviations calculated over the averaging windows range between: 0.4–2.5 ‰ for δD (with mean 0.9 ‰), 0.15–0.50 ‰ for δ^{18}O (with mean 0.25 ‰) and 10–400 ppmv for humidity level (with mean 65 ppmv). The drift between calibrations was assumed to be linear.

During the first two winter months, the humidity level at which calibrations were performed was manually decreased to ~ 4000 ppmv in order to reach a level close to the ambient air humidity. However, the instrumental noise induced a loss of accuracy in the calibrations (as reported in Sect. 3.3). We therefore set the humidity level back to ~ 12 000 ppmv.

Overall, the analyzer drift during the one-year period was < 2 ‰ for δD and < 0.5 ‰ for δ^{18}O, resulting in V-SMOW slope change < 0.015 for δD and < 0.03 for δ^{18}O.

3.5 Instrument accuracy

Steen-Larsen et al. (2013) conservatively estimated the instrument uncertainty, when calibration was working properly, to be 1.4 ‰ for δD and 0.23 ‰ for δ^{18}O at humidity levels between 1500 and 6000 ppmv, respectively. Following Steen-Larsen et al. we assume that we have similar precision and accuracy at these humidity levels and conservatively decide to use them for higher humidity levels.

At lower humidity levels we observe an increase of the uncertainty in our measurements (see Fig. 3, red and black error bars) by a factor 4 at 1000 ppmv and a factor 8 at

AMTD
7, 475–507, 2014

500 ppmv. We therefore estimate the uncertainty to be between 1000 and 1500 ppmv to be 5.6 ‰ for δD and 0.92 ‰ for δ^{18}O and between 500 and 1000 ppmv to be 11.2 ‰ for δD and 1.84 ‰ for δ^{18}O. We therefore decided not to report any measurements for values below 500 ppmv.

Such low humidity levels are encountered at Kourovka during winter. In total, 16 % of all hourly measurements have been made at humidity levels < 1500 ppmv (42 % of the winter measurements) and 2.5 % of the measurements have been made at humidity levels < 500 ppmv (6.4 % of the winter measurements).

3.6 Hourly observations time-series

The hourly averaged Picarro humidity and isotopic data and Gill meteorological data are presented in Fig. 5, after applying all the corrections and calibrations discussed in the previous sections.

Humidity concentration varies from ~ 250 ppmv in winter up to ~ 23 000 ppmv in summer, and co-varies with local surface air temperature. The seasonal cycle of δD and δ^{18}O is parallel with the seasonal cycle of humidity and temperature, with the respective ranges of variation being −103 ‰ to −300 ‰ and −14 ‰ to −39 ‰. Maximum values are observed in summer (August), and minimum values in winter (January).

In addition to the seasonal pattern, significant variations are observed on a timescale of several days with respective magnitudes of 3000–8000 ppmv, 50–100 ‰, 10–15 ‰ and 2–8 ‰ in humidity, δD, δ^{18}O and d-excess.

Deuterium excess values are only reported after September 2012, due to the instabilities in the calibrations during the first months of measurement. They show a lagged seasonal cycle, with maximum values in winter (~ 20 ‰) and minimum values in summer (~ 5 ‰ during the day and ~ −25 ‰ during the night). On a day-to-day basis, deuterium excess variations have a magnitude of less than 3 %. However, the summer deuterium excess variability is very large at the diurnal scale; this feature is further investigated in Sect. 3.9.

AMTD
7, 475–507, 2014

Our observed seasonal cycle is consistent with earlier results obtained from north-east Siberia precipitation data by Kurita (2011). His record shows the peak $\delta^{18}O$ occurring in late summer, and the minimum in mid-winter; his d-excess values decrease strongly during summer months, also reaching negative values. However, the maximum d-excess values were observed during mid-autumn – a feature which does not appear in our 2012 record. Extending the Kourovka record over several years would allow the average seasonal cycle to be established.

3.7 δD vs. δ^{18}O

Figure 6 shows the relationship between surface vapour δD and $\delta^{18}O$ through the complete campaign time period (left panel) and for each season (right panels). Fitted parameters are presented in Table 2. Here and after, seasons are defined as follows (based on Kourovka climate): 21 September–27 November (Autumn, $N = 1362$), 28 November–31 March (Winter, $N = 2619$), 1 April–31 May (Spring, $N = 1101$) and 1 June–31 August (Summer, $N = 1705$).

The linear slope fitted through all the measurements (red and green dots on Fig. 6) equals 7.5 for the whole data set and varies for different seasons from the maximum value (7.7) in winter to the minimum value (5.6) in summer (solid lines on Fig. 6). For all seasons, strong coefficients of determination are observed ($R^2 > 0.94$), with the exception of summer where the coefficient of determination is smaller ($R^2 = 0.76$).

As we observe strong diurnal cycles in the measurements time-series, the relationship between δD and $\delta^{18}O$ have been analyzed separately for the daytime measurements. For this we take the measurements performed during the daytime period from 12 to 21 h of local time, which is free from strong variability (red dots on Fig. 6). We observe significant change of the slope for spring (7.2) and summer (7.0) (dashed lines on Fig. 6) with higher coefficients of determination ($R^2 > 0.95$). The overall value of the slope for the daytime measurements equals 7.7. These results point out the significant role of local processes during the warm seasons in this region indicating a possible influence of continental recycling.

AMTD
7, 475–507, 2014

3.8 δD vs. local meteorological data (humidity and temperature)

Figure 7 shows interdependencies of isotopic composition (δD) and meteorological data (temperature and humidity) for the full data set (left panels) and for each season (right panels) with fitted parameters presented in Table 3.

For δD, the strongest correlations are observed with the logarithm-of-humidity, which is consistent with what is expected from Rayleigh distillation. We report R^2 = 0.88 for all data, about 0.6 for autumn and winter, and 0.3–0.4 in spring and summer. The slopes are changing from 52 to 26 ‰ per log(humidity [ppmv]); the weakest ones can also be seen to occur in spring and summer.

A strong relationship is also observed between δD and temperature, as expected from the close relationship between temperature and logarithm-of-humidity, albeit less strong than the correlation with logarithm-of-humidity. We report R^2 = 0.84 for all data, about 0.6 for autumn and winter and much lower for spring and summer (0.15). The overall relationship has a slope of 3.1 ‰ $^{\circ}C^{-1}$, with even lower isotope-temperature slopes in spring (1.0 ‰ $^{\circ}C^{-1}$) and summer (0.9 ‰ $^{\circ}C^{-1}$). We note that this slope is about half the relationship expected from Rayleigh distillation.

The data indicate that while local temperature is a key driver of autumn-winter seasonal variations of δD, due to temperature-driven distillation effects, this is not the case for spring-summer. During these seasons, the data depict a persistent but weaker relationship with logarithm-of-humidity (accounting for about 30 % of the variance), and a minor impact of temperature. We conclude that in spring-summer local processes controlling local humidity variations are independent of surface temperature and probably related to continental recycling and local evapotranspiration (Welp et al., 2012; Berkelhammer et al., 2013), or convective activity.

3.9 Diurnal variations

The period from May to September is characterized by the frequent occurrence of days with a strong diurnal d-excess cycle, which is not seen during other seasons (Fig. 5).

AMTD
7, 475–507, 2014

This diurnal variability arises from small variations in humidity (1000–3000 ppmv) and $\delta^{18}O$ (1–5 ‰), but with no counterpart in δD. This diurnal decoupling between δD and $\delta^{18}O$ contrasts with the overall strong correlation depicted at the daily to seasonal scale (Fig. 6).

The stacked diurnal cycles for d-excess and humidity for the period from 8 May 2013 till 31 August 2013 (95 days with full diurnal cycles) are shown in Fig. 8 (left panels). The yellow bars on the figures show the time of sunrise (changing between 05:12 local time, hereafter LT, on 8 May and 07:05 LT on 31 August) and similarly the dark red bars show sunset (changing between 21:07 LT on 8 May and 23:03 LT on 31 August). Following the analysis of Berkelhammer et al. (2013), we observe two distinct patterns in d-excess and humidity, which are classified using an objective cluster analysis (SciPy k-means clustering routines). The red line (Cluster 1, 43 cycles) and the blue line (Cluster 2, 52 cycles) on the right panels of Fig. 8 indicate the mean values of each cluster, with corresponding standard deviations shown by shading. These two clusters show similar variability during the day, but differ by the magnitude of d-excess night depletion (decrease of 21 ‰ and 7 ‰, respectively), related to the magnitude of the daily humidity peak level (increase of 2400 and 1000 ppmv, respectively). The difference between the minimum d-excess values of the clusters (15 ‰) is 2.9 times larger than the standard deviation of Cluster 1.

This d-excess variability is similar to that reported by Berkelhammer et al. (2013), albeit they seem to only observe clusters similar to Cluster 1 and not Cluster 2. This difference can be explained by the fact that our measurements are carried out in a clearing of size 100 × 100 metres and surrounded by very dense natural forest, while the measurements of Berkelhammer et al. were carried out inside a mature open canopy (LAI = 1.9) ponderosa pine forest. Similar d-excess diurnal cycles had also been reported by Welp et al. (2012) in the meta-analysis of water vapour measurements from six different sites located in various ecosystems (forest, grassland, agricultural and urban settings), all of which showed the general feature of d-excess midday increase with remarkably similar phases in the time progression. Throughout all the studies mentioned, the magnitude

AMTD
7, 475–507, 2014

of d-excess daily variations ranges from ∼ 5 ‰ to ∼ 20 ‰ from site to site, but all share the same timing (decrease during the evening and the night with more rapid recovery in the morning).

Within all the diurnal cycles from Fig. 6, an inverse correlation is observed between the d-excess value decrease in the early morning and the humidity value increase during the morning burst ($R = -0.45$, $p > 0.9999$). This finding is consistent with the mechanism proposed by Berkelhammer et al. (2013) whereby the diurnal d-excess cycle is a result of dew-fall and vapour-liquid interaction within the canopy. The morning burst is caused by initiation of transpiration and one would therefore expect an inverse relationship between the strength of the diurnal d-excess cycle and the increase in humidity during the morning burst.

4 Conclusions and perspectives

This study reports the successful use of a Picarro Inc. water vapour CRDS-analyzer for atmospheric water vapour isotope measurements at the surface in Western Siberia (Kourovka, Russia). A calibration protocol had been developed to apply humidity and drift corrections and to present the measurements on the V-SMOW scale. Overall, the instrument demonstrated its ability to produce reliable measurements with an overall drift of less than 2 ‰ and 0.5 ‰ for δD and δ^{18}O, respectively. Frequent calibrations (every six hours) reveal a good reproducibility with standard deviations of 0.9 ‰ and 0.25 ‰ for δD and δ^{18}O, respectively.

At low humidity concentrations the measurements are subject to large errors. In particular, the Picarro Standards Delivery Module requires further optimization if it is to give reasonable calibration results for humidity levels below 4000 ppmv. We demonstrate that using dry air instead of DRIERITE produces excellent reproducibility for the isotope-humidity calibration curve established when using different standards.

Our data set reveals considerable seasonal variations of isotopic composition and humidity concentration with a strong dependency on weather conditions. The strongest

AMTD
7, 475–507, 2014

links are observed between δD and logarithm-of-humidity, and with temperature. However, these relationships are much weaker in spring-summer, especially for temperature.

The summer period shows a strong diurnal variability of d-excess, which was not seen during other seasons. This variability has a distinct relationship with sunset and sunrise and is consistent with interactions of dew-fall and canopy liquids with the atmospheric water vapour isotopes. During the nighttime, d-excess experiences a strong decrease to negative values with the minimum occurring close to sunrise, after which it returns to the value affected by synoptic variability. By means of objective cluster analysis, two dominant patterns for d-excess and humidity daily cycles are distinguished. An inverse relationship is observed between the strength of the d-excess cycle and the morning humidity increase.

The data obtained in this study provide a firm basis for further research of the atmospheric hydrological cycle of Western Siberia. They are now available for comparison with remote sensing measurements, outputs from moisture trajectory calculations, simulations of water vapour isotopic composition from land surface and boundary-layer models, or atmospheric general circulation models.

The work is part of a project investigating the water and carbon cycles in the permafrost and pristine peatlands of Western Siberia and their projected changes under global warming. The full data set of isotopic and meteorological measurements discussed in this paper is available on the official site of the project WSibIso ("Impact of climate change on water and carbon cycles of melting permafrost of Western Siberia"): http://www.wsibiso.ru, and in the Web database of water isotope monitoring data: http://waterisotopes.lsce.ipsl.fr.

Acknowledgements. This research was supported by the grant of the Russian government under the contract 11.G34.31.0064. The authors thank John Gash for valuable edits of this manuscript.

AMTD
7, 475–507, 2014

The publication of this article is financed by CNRS-INSU.

References

Aemisegger, F., Sturm, P., Graf, P., Sodemann, H., Pfahl, S., Knohl, A., and Wernli, H.: Measuring variations of $\delta_{18}O$ and δ_2H in atmospheric water vapour using two commercial laser-based spectrometers: an instrument characterisation study, Atmos. Meas. Tech., 5, 1491–1511, doi:10.5194/amt-5-1491-2012, 2012.

Aemisegger, F., Pfahl, S., Sodemann, H., Lehner, I., Seneviratne, S. I., and Wernli, H.: Deuterium excess as a proxy for continental moisture recycling and plant transpiration, Atmos. Chem. Phys. Discuss., 13, 29721–29784, doi:10.5194/acpd-13-29721-2013, 2013.

Baer, D. S., Paul, J. B., Gupta, M., and O'Keefe, A.: Sensitive absorption measurements in the near-infrared region using off-axis integrated-cavity output spectroscopy, Appl. Phys. B-Lasers O., 75, 261–265, 2002.

Barkan, E. and Luz, B.: Diffusivity fractionations of $H_2{}^{16}O/H_2{}^{17}O$ and $H_2{}^{16}O/H_2{}^{18}O$ in air and their implications for isotope hydrology, Rapid Commun. Mass Sp., 21, 2999–3005, doi:10.1002/rcm.3180, 2007.

Berkelhammer, M., Hu, J., Bailey, A., Noone, D. C., Still, C. J., Barnard, H., Gochis, D., Hsiao, G. S., Rahn, T., and Turnipseed, A.: The nocturnal water cycle in an open-canopy forest, J. Geophys. Res.-Atmos., 118, 10225–10242, doi:10.1002/jgrd.50701, 2013.

Bonne, J.-L., Masson-Delmotte, V., Cattani, O., Delmotte, M., Risi, C., Sodemann, H., and Steen-Larsen, H. C.: The isotopic composition of water vapour and precipitation in Ivittuut, Southern Greenland, Atmos. Chem. Phys. Discuss., 13, 30521–30574, doi:10.5194/acpd-13-30521-2013, 2013.

Brand, W. A., Geilmann, H., Crosson, E. R., and Rella, C. W.: Cavity ring-down spectroscopy versus high-temperature conversion isotope ratio mass spectrometry; a case study on δ^2H

AMTD
7, 475–507, 2014

and $\delta^{18}O$ of pure water samples and alcohol/water mixtures, Rapid Commun. Mass Sp., 23, 1879–1884, doi:10.1002/rcm.4083, 2009.
Ciais, P. and Jouzel, J.: Deuterium and oxygen 18 in precipitation: isotopic model, including mixed cloud processes, J. Geophys. Res.-Atmos., 99, 16793–16803, 1994.
Craig, H.: Standard for reporting concentrations of deuterium and oxygen-18 in natural waters, Science, 133, 1833–1834, 1961.
Craig, H. and Gordon, L.: Deuterium and oxygen-18 variations in the ocean and marine atmosphere, in: Stable Isotopes in Oceanography Studies and Paleotemperatures, 26–30 July 1965, Spoleto, Italy, 1965.
Crosson, E. R., Ricci, K. N., Richman, B. A., Chilese, F. C., Owano, T. G., Provencal, R. A., Todd, M. W., Glasser, J., Kachanov, A. A., Paldus, B. A., Spence, T. G., and Zare, R. N.: Stable isotope ratios using cavity ring-down spectroscopy: Determination of $^{13}C/^{12}C$ for carbon dioxide in human breath, Anal. Chem., 74, 2003–2007, doi:10.1021/ac025511d, 2002.
Dansgaard, W.: Stable isotopes in precipitation, Tellus, 16, 436–468, doi:10.1111/j.2153-3490.1964.tb00181.x, 1964.
Ellehoj, M. D., Steen-Larsen, H. C., Johnsen, S. J., and Madsen, M. B.: Ice-vapor equilibrium fractionation factor of hydrogen and oxygen isotopes: experimental investigations and implications for stable water isotope studies, Rapid Commun. Mass Sp., 27, 2149–2158, doi:10.1002/rcm.6668, 2013.
Farlin, J., Lai, C.-T., and Yoshimura, K.: Influence of synoptic weather events on the isotopic composition of atmospheric moisture in a coastal city of the western United States, Water Resour. Res., 49, 3685–3696, doi:10.1002/wrcr.20305, 2013.
Farquhar, G. D., Cernusak, L. A., and Barnes, B.: Heavy water fractionation during transpiration, Plant Physiol., 143, 11–18, 2007.
Field, R. D., Jones, D. B. A., and Brown, D. P.: Effects of postcondensation exchange on the isotopic composition of water in the atmosphere, J. Geophys. Res.-Atmos., 115, D24305, doi:10.1029/2010JD014334, 2010.
Galewsky, J., Rella, C., Sharp, Z., Samuels, K., and Ward, D.: Surface measurements of upper tropospheric water vapor isotopic composition on the Chajnantor Plateau, Chile, Geophys. Res. Lett., 38, L17803, doi:10.1029/2011GL048557, 2011.
Gat, J. R.: Oxygen and hydrogen isotopes in the hydrological cycle, Annu. Rev. Earth Pl. Sc., 24, 225–262, 1996.

AMTD
7, 475–507, 2014

Gonfiantini, R.: Standards for stable isotope measurements in natural compounds, Nature, 271, 534–536, 1978.

Gribanov, K., Jouzel, J., Bastrikov, V., Bonne, J.-L., Breon, F.-M., Butzin, M., Cattani, O., Masson-Delmotte, V., Rokotyan, N., Werner, M., and Zakharov, V.: ECHAM5-wiso water vapour isotopologues simulation and its comparison with WS-CRDS measurements and retrievals from GOSAT and ground-based FTIR spectra in the atmosphere of Western Siberia, Atmos. Chem. Phys. Discuss., 13, 2599–2640, doi:10.5194/acpd-13-2599-2013, 2013.

Gupta, P., Noone, D., Galewsky, J., Sweeney, C., and Vaughn, B. H.: Demonstration of high-precision continuous measurements of water vapor isotopologues in laboratory and remote field deployments using wavelength-scanned cavity ring-down spectroscopy (WS-CRDS) technology, Rapid. Commun. Mass. Sp., 23, 2534–2542, 2009.

Han, L.-F., Groening, M., Aggarwal, P., and Helliker, B. R.: Reliable determination of oxygen and hydrogen isotope ratios in atmospheric water vapour adsorbed on 3A molecular sieve, Rapid. Commun. Mass. Sp., 20, 3612–3618, doi:10.1002/rcm.2772, 2006.

Jacob, H. and Sonntag, C.: An 8-year record of the seasonal variation of ^{2}H and ^{18}O in atmospheric water vapour and precipitation at Heidelberg, Germany, Tellus B, 43, 291–300, 1991.

Kerstel, E. R. T. and Gianfrani, L.: Advances in laser-based isotope ratio measurements: selected applications, Appl. Phys. B-Lasers O., 92, 439–449, 2008.

Kerstel, E. R. T., van Trigt, R., Dam, N., Reuss, J., and Meijer, H. A. J.: Simultaneous determination of the $^{2}H/^{1}H$, $^{17}O/^{16}O$, and $^{18}O/^{16}O$ isotope abundance ratios in water by means of laser spectrometry, Anal. Chem., 71, 5297–5303, 1999.

Kurita, N.: Origin of Arctic water vapor during the ice-growth season, Geophys. Res. Lett., 38, L02709, doi:10.1029/2010GL046064, 2011.

Kurita, N., Yoshida, N., Inoue, G., and Chayanova, E. A.: Modern isotope climatology of Russia: a first assessment, J. Geophys. Res.-Atmos., 109, D03102, doi:10.1029/2003JD003404, 2004.

Kurita, N., Newman, B. D., Araguas-Araguas, L. J., and Aggarwal, P.: Evaluation of continuous water vapor δD and δ_{18}O measurements by off-axis integrated cavity output spectroscopy, Atmos. Meas. Tech., 5, 2069–2080, doi:10.5194/amt-5-2069-2012, 2012.

Majoube, M.: Fractionnement en oxygène 18 et en deutérium entre l'eau et sa vapeur, J. Chim. Phys., 68, 1423–1436, 1971.

AMTD
7, 475–507, 2014

Merlivat, L.: Molecular diffusivities of $H_2{}^{16}O$, $HD^{16}O$ and $H_2{}^{18}O$ in gases, J. Chem. Phys., 69, 2864–2871, 1978.
Merlivat, L. and Jouzel, J.: Global climatic interpretation of the deuterium-oxygen 18 relationship for precipitation, J. Geophys. Res.-Oceans, 84, 5029–5033, doi:10.1029/JC084iC08p05029, 1979.
Merlivat, L. and Nief, G.: Fractionnement isotopique lors des changements d'état solide-vapeur et liquide-vapeur de l'eau à des températures inférieures à 0 °C, Tellus, 19, 122–127, doi:10.1111/j.2153-3490.1967.tb01465.x, 1967.
Rozanski, K., Araguás-Araguás, L., and Gonfiantini, R.: Isotopic patterns in modern global precipitation, in: Geophraphical Monograph Series, edited by: Swart, P. K., Lohmann, K. C., McKenzie, J., and Savin, S., Vol. 78, American Geophysical Union, Washington DC, 1–36, 1993.
Shalaumova, Y. V., Fomin, V. V., and Kapralov, D. S.: Spatiotemporal dynamics of the Urals climate in the second half of the 20th century, Russ. Meteorol. Hydrol., 35, 107–114, 2010.
Steen-Larsen, H. C., Johnsen, S. J., Masson-Delmotte, V., Stenni, B., Risi, C., Sodemann, H., Balslev-Clausen, D., Blunier, T., Dahl-Jensen, D., Ellehøj, M. D., Falourd, S., Grindsted, A., Gkinis, V., Jouzel, J., Popp, T., Sheldon, S., Simonsen, S. B., Sjolte, J., Steffensen, J. P., Sperlich, P., Sveinbjörnsdóttir, A. E., Vinther, B. M., and White, J. W. C.: Continuous monitoring of summer surface water vapor isotopic composition above the Greenland Ice Sheet, Atmos. Chem. Phys., 13, 4815–4828, doi:10.5194/acp-13-4815-2013, 2013.
Strong, M. Z. D., Sharp, D., and Gutzler, D. S.: Diagnosing moisture transport using D/H ratios of water vapor, Geophys. Res. Lett., 34, L03404, doi:10.1029/2006GL028307, 2007.
Sturm, P. and Knohl, A.: Water vapor δ_2H and δ_{18}O measurements using off-axis integrated cavity output spectroscopy, Atmos. Meas. Tech., 3, 67–77, doi:10.5194/amt-3-67-2010, 2010.
Tremoy, G., Vimeux, F., Cattani, O., Mayaki, S., Souley, I., and Favreau, G.: Measurements of water vapor isotope ratios with wavelength-scanned cavity ring-down spectroscopy technology: new insights and important caveats for deuterium excess measurements in tropical areas in comparison with isotope-ratio mass spectrometry, Rapid Commun. Mass Sp., 25, 3469–3480, doi:10.1002/rcm.5252, 2011.
Tremoy, G., Vimeux, F., Mayaki, S., Souley, I., Cattani, O., Risi, C., Favreau, G., and Oi, M.: A 1-year long ^{18}O record of water vapor in Niamey (Niger) reveals insight-

AMTD
7, 475–507, 2014

ful atmospheric processes at different timescales, Geophys. Res. Lett., 39, L08805, doi:10.1029/2012GL051298, 2012

Uemura, R., Matsui, Y., Yoshimura, K., Motoyama, H., and Yoshida, N.: Evidence of deuterium excess in water vapor as an indicator of ocean surface conditions, J. Geophys. Res.-Atmos., 113, D19114, doi:10.1029/2008JD010209, 2008.

Welp, L. R., Lee, X., Griffis, T. J., Wen, X.-F., Xiao, W., Li, S., Sun, X., Hu, Z., Martin, M. V., and Huang, J.: A meta-analysis of water vapor deuterium-excess in the midlatitude atmospheric surface layer, Global Biogeochem. Cy., 26, GB3021, doi:10.1029/2011GB004246, 2012.

AMTD

7, 475–507, 2014

Table 1. Humidity correction functions and coefficients for DW and YEKA standards.

N	Standard	Isotope	Function	*a*	*b*
1	DW	δ^{18}O	$y = a \cdot \exp(-x/b)$	0.952 ± 0.153	1863 ± 344
2	(with DRIERITE)	δD	$y = a + b/x$	0.820 ± 0.107	$-13\,160 \pm 315$
3	YEKA	δ^{18}O	$y = a \cdot \exp(-x/b)$	3.770 ± 0.157	1653 ± 79
4	(with DRIERITE)	δD	$y = a \cdot \exp(-x/b)$	6.224 ± 0.480	3270 ± 322
5	DW & YEKA	δ^{18}O	$y = a \cdot \exp(-x/b)$	8.394 ± 0.123	551.0 ± 11.3
6	(with dry gas)	δD	$y = a \cdot \exp(-x/b)$	-26.98 ± 3.80	140.4 ± 13.2

AMTD
7, 475–507, 2014

Table 2. δD vs. δ^{18}O (linear fit parameters for hourly averaged data).

Period	N	Slope	Intercept	R^2
All data	6787	7.49 ± 0.01	-1.94 ± 0.27	0.99
All data (daytime)	2542	7.74 ± 0.01	6.75 ± 0.30	0.99
Autumn	1362	7.20 ± 0.03	-5.78 ± 0.65	0.98
Winter	2619	7.73 ± 0.02	4.40 ± 0.78	0.98
Spring	1101	6.85 ± 0.05	-14.3 ± 1.2	0.94
Spring (daytime)	408	7.24 ± 0.06	-3.55 ± 1.28	0.98
Summer	1705	5.57 ± 0.07	-39.6 ± 1.4	0.76
Summer (daytime)	634	7.02 ± 0.06	-7.74 ± 1.22	0.95

AMTD
7, 475–507, 2014

Table 3. δD vs. meteorological data (logarithm-of-humidity and temperature) (linear fit parameters for hourly averaged data).

Period	N	δD vs. logarithm-of-humidity			δD vs. temperature		
		Slope	Intercept	R^2	Slope	Intercept	R^2
All data	6787	44.3 ± 0.2	-566 ± 2	0.88	3.06 ± 0.02	-197 ± 0.3	0.84
Autumn	1362	52.2 ± 1.2	-634 ± 10	0.59	3.19 ± 0.08	-189 ± 0.6	0.60
Winter	2619	29.7 ± 0.4	-464 ± 3	0.65	2.23 ± 0.04	-215 ± 0.6	0.56
Spring	1101	35.9 ± 1.3	-480 ± 11	0.42	–	–	0.16
Summer	1705	26.5 ± 0.9	-397 ± 8	0.35	–	–	0.15

AMTD
7, 475–507, 2014

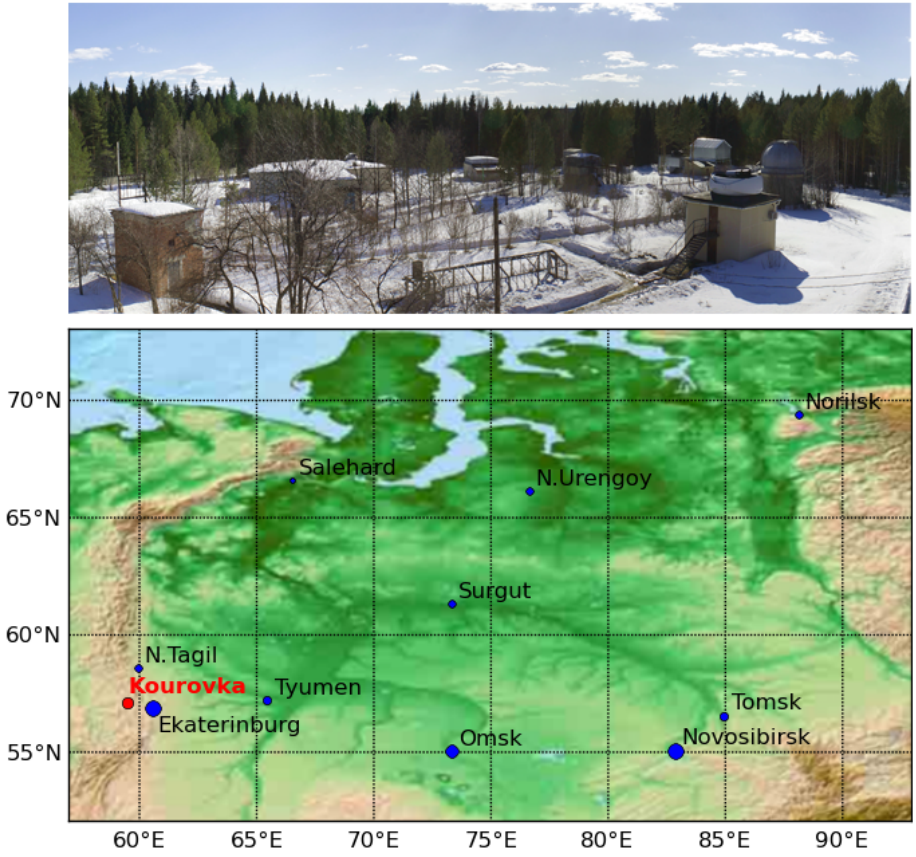

Fig. 1. Top to bottom: view of Kourovka astronomical observatory, map of Western Siberia (from the Ural Mountains on the west to the river Yenisei on the east) showing the location of major cities (blue circles) and the observatory (red circle).

AMTD
7, 475–507, 2014

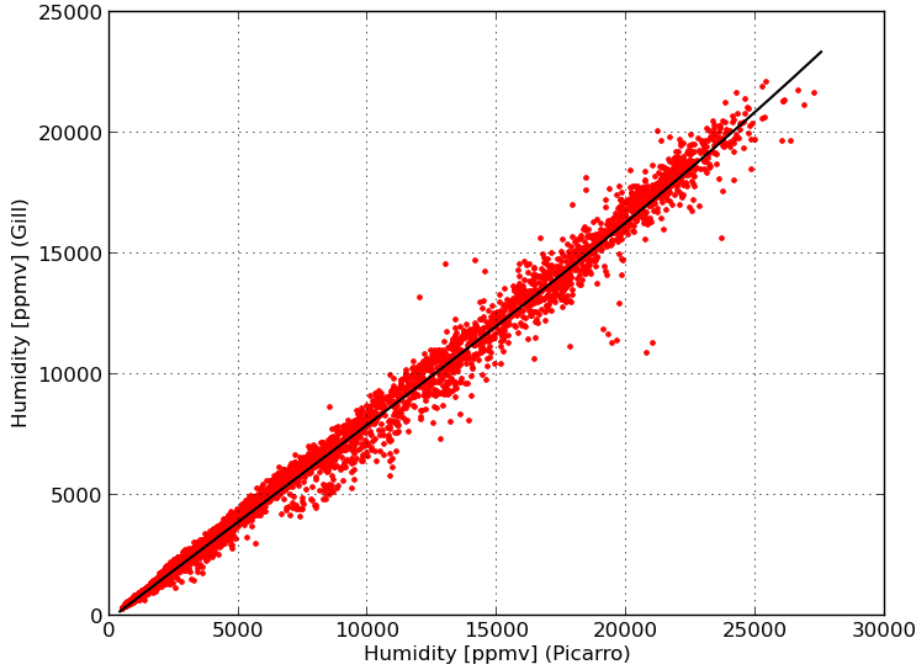

Fig. 2. Humidity measurements: Meteorological sensor (Gill Instruments) vs. Picarro. Black curve: third degree polynomial regression (Eq. 3).

AMTD
7, 475–507, 2014

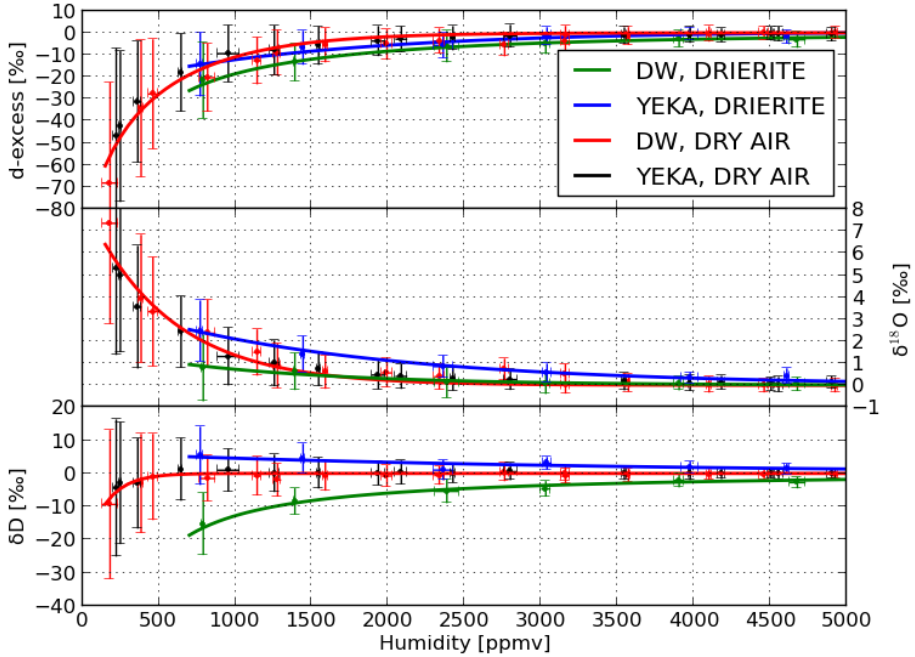

Fig. 3. Picarro humidity–isotope response functions. Green error bars: calibration performed using DW standard and DRIERITE column, blue error bars: calibration performed using YEKA standard and DRIERITE column, red error bars: calibration performed using DW standard and dry gas, black error bars: calibration performed using YEKA standard and dry gas. Solid lines represent linear fits to the data. For the measurements of DW and YEKA standards using dry air one conjoint fitting line is shown in red.

AMTD
7, 475–507, 2014

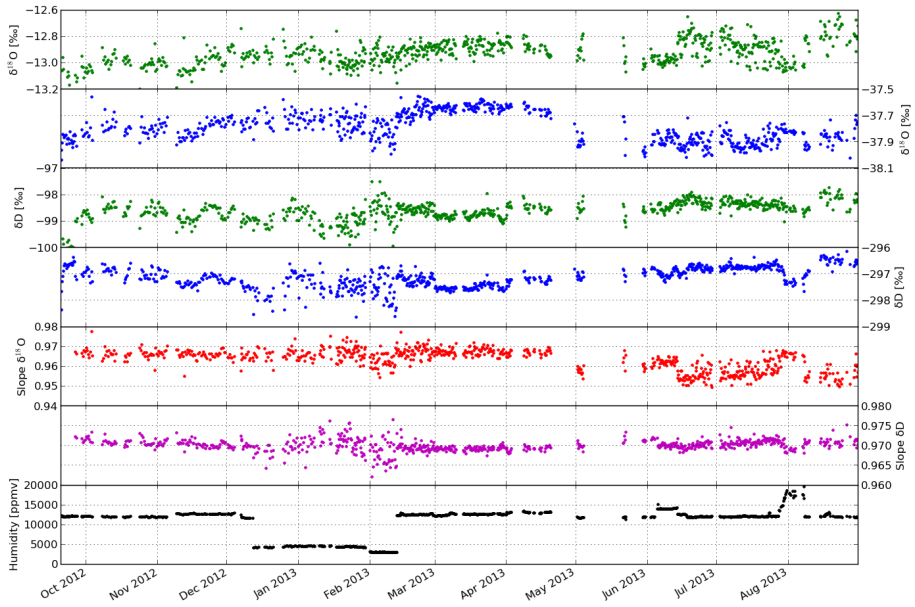

Fig. 4. Picarro calibration data. Top to bottom: measured δ^{18}O and δD values in ‰ for DW standard (green dots) and YEKA standard (blue dots), calculated calibration slope for δ^{18}O measurements (red dots) and δD measurements (purple dots), humidity concentration in ppmv (black dots).

AMTD
7, 475–507, 2014

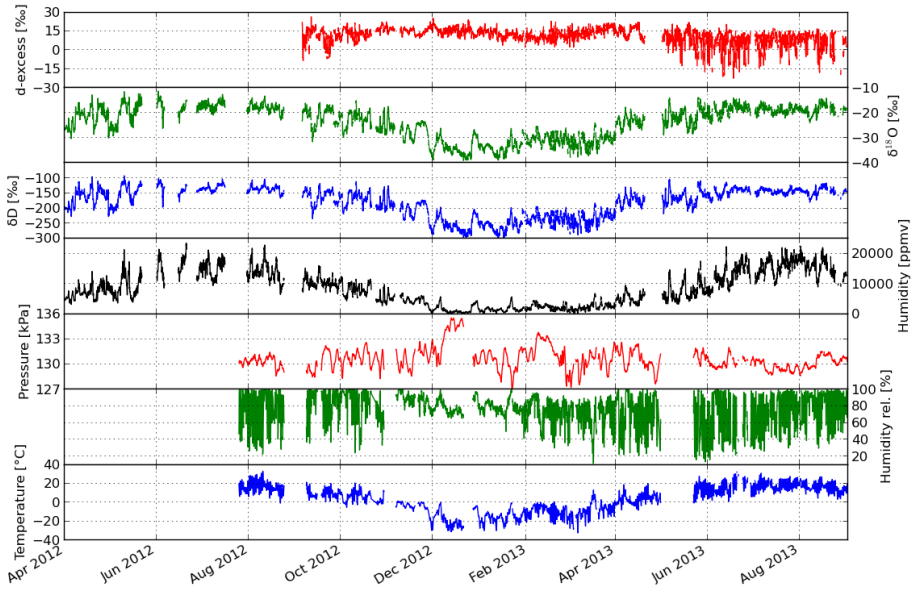

Fig. 5. Isotopic and meteorological measurements at Kourovka site. Top to bottom: d-excess, δ^{18}O and δD in ‰, humidity concentration in ppmv, pressure in kPa, relative humidity in %, and temperature in ˚C. Deuterium excess values are not reported before September 2012, due to instabilities of calibrations during this period.

AMTD
7, 475–507, 2014

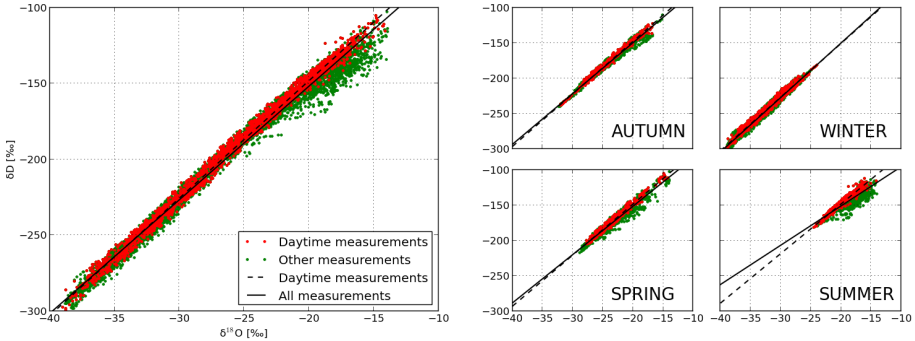

Fig. 6. δD vs. δ^{18}O. Left panel: all measurements, right panels: seasonal measurements, red dots: daytime measurements (from 12:00 to 21:00 LT), green dots: all other measurements, dashed line: linear fit through daytime measurements of the graph, solid line: linear fit through all measurements of the graph. See Table 2 for calculations of determination coefficients and slopes.

AMTD
7, 475–507, 2014

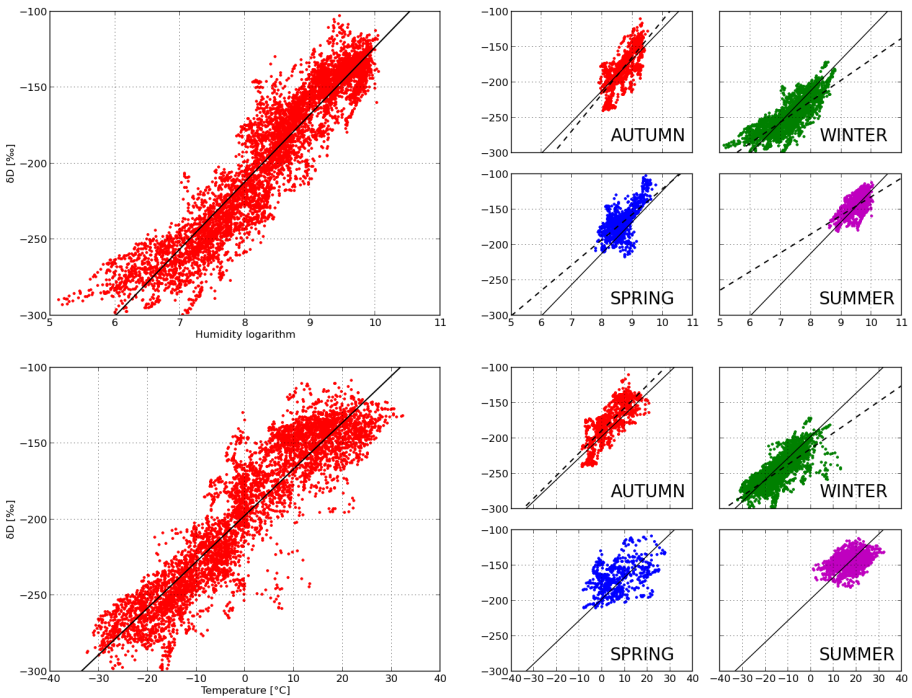

Fig. 7. δD vs. logarithm-of-humidity (top) and δD vs. temperature (bottom). Left panels: all measurements, right panels: seasonal measurements, solid line: linear fit through all measurements, dashed line: linear fit through seasonal measurements. See Table 3 for calculations of determination coefficients and slopes.

AMTD
7, 475–507, 2014

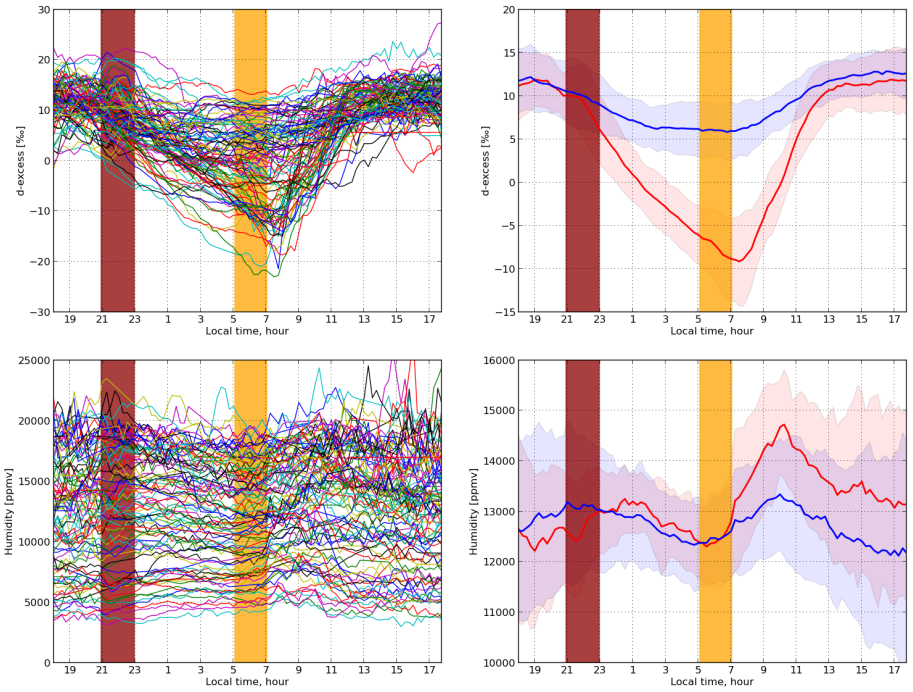

Fig. 8. Diurnal cycles for d-excess (top) and humidity (bottom). Left panels: all diurnal cycles, right panels: two dominant clusters, yellow bars: sunrise time, dark red bars: sunset time. The shading shows the standard deviation for each cluster.

AMTD
7, 475–507, 2014